Creating Ti–Fe α/β Alloys by Diffusion-Driven Solid-State Processing

XU, Jiaqi, ZHANG, Xub, DONOGHUE, Jack M., SMITH, Albert D., UNNIKRISHNAN, Rahul, THOMAS, Rhys, NEKOUIE, Vahid, LUO, J., HU, Dongchen, PREUSS, Michael and WITHERS, Philip J.

Advanced Engineering Materials

ADVANCED ENGINEERING MATERIALS
www.aem-journal.com

RESEARCH ARTICLE OPEN ACCESS

Creating Ti–Fe α/β Alloys by Diffusion-Driven Solid-State Processing

Jiaqi Xu[1] | Xun Zhang[1] | Jack M. Donoghue[1] | Albert D. Smith[2] | Rahul Unnikrishnan[1] | Rhys Thomas[1] | Vahid Nekouie[3] | Jie Luo[4] | Dongchen Hu[1] | Michael Preuss[1,4] | Philip J. Withers[1,4]

[1]Henry Royce Institute, Department of Materials, University of Manchester, Manchester, UK | [2]TESCAN-UK, Cambridge, UK | [3]School of Engineering and Built Environment, Sheffield Hallam University, Sheffield, UK | [4]Department of Materials Science and Engineering, Monash University, Clayton, Victoria, Australia

Correspondence: Philip J. Withers (p.j.withers@manchester.ac.uk)

Received: 7 November 2025 | **Revised:** 11 February 2026 | **Accepted:** 17 February 2026

Keywords: diffusion | microstructure | powder metallurgy | processing

ABSTRACT

Some alloys are difficult to make by ingot metallurgy. Here, the potential for making alloys by hot isostatic pressing (HIPing) and homogenising powder mixtures is explored for Ti–Fe. Iron is an effective and cost-effective β stabiliser but gives rise to segregation issues during solidification. Exploiting the fact that Fe diffusion through Ti is fast, Fe and Ti powders are co-HIPed at, and homogenised at, only 800°C in order to create an α+β microstructure based on small prior β grains. The evolution of phase composition and elemental distribution during homogenisation has been tracked quantitatively in 3D by X-ray computed tomography and in 2D by energy dispersive spectroscopy and electron backscatter diffraction. The final homogenised microstructure consists of fine α Ti laths separated by β ligaments with a prior β grain size of only 80 μm, free of TiFe intermetallics with no indication of a grain boundary α constituent. Kirkendall pore formation was observed during homogenisation heat treatment due to the fast diffusion of Fe in Ti. This study shows the potential of HIP processing followed by homogenisation heat treatment as a novel solid-state manufacturing route for difficult-to-cast alloys.

1 | Introduction

α+β Ti alloys are widely used for a variety of chemical, biomedical and structural applications due to their potential for high specific strength, excellent corrosion resistance, good biocompatibility, high chemical stability and good formability [1]. Alloying elements are commonly used to stabilise some fraction of the high-temperature β-phase relative to the low temperature α-phase upon cooling to room temperature. This can be achieved by adding isomorphous (V, Mo, Nb, Ta) or eutectoid (Fe, Cr, Cu, Co) β-stabilising elements [1].

Out of the various β-stabilisers, Fe is the cheapest alloying element, while also being a strong β-phase stabiliser [2–6]. According to the binary Ti–Fe phase diagram (Figure 1), the β phase decomposes into α phase and TiFe intermetallic (ordered B2 phase) via a eutectoid reaction at 15.4 wt.% Fe and 583°C [1]. These intermetallic-containing alloys have been shown to exhibit high yield strength (>1.8 GPa) and reasonable ductility (>6%) [8, 9]. Recently, a binary Ti–Fe superalloy has been proposed by homogenisation in the β phase field followed by ageing at a temperature slightly above the eutectoid temperature to promote the TiFe (β') precipitation strengthening in the parent β-phase [8]; however, three phase (including Ti_2Fe) microstructures have proven difficult to avoid [10]. Gussone et al. produced ultrafine eutectic Ti-32.5Fe alloys using laser powder bed fusion additive manufacturing. The alloy has high compressive yield strength at 600°C [11]. In large-scale production, Ti–Fe binary alloys often suffer from severe chemical segregation during ingot metallurgy, as well as forming large β-grain flecks, which are detrimental to the mechanical performance [8, 12–14]. Previous studies [15, 16] have also indicated that additions of Fe over 2.5 wt.% in titanium alloys might lead to Fe segregation and porosity due to the eutectoid reaction and the Kirkendall porosity, respectively.

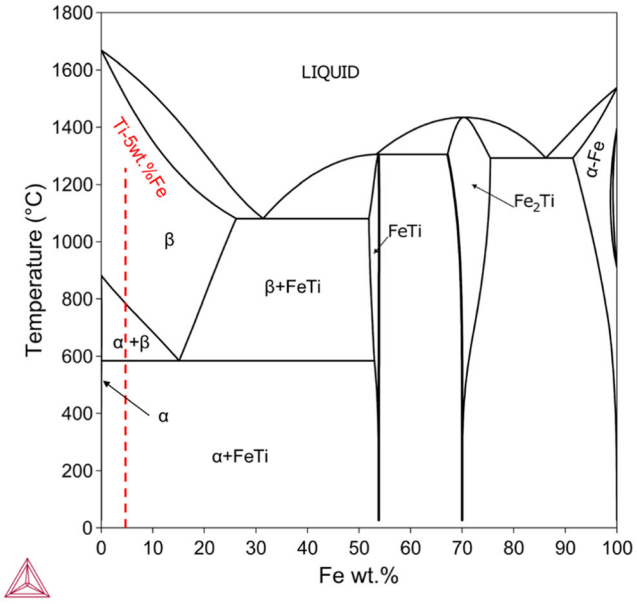

FIGURE 1 | The Ti–Fe phase diagram calculated with the TCBIN database in Thermo-Calc Software [7].

It has long been realised that, as illustrated in Figure 2, Fe is extremely mobile in titanium, exhibiting a diffusion coefficient in α-Ti that is six orders of magnitude higher than Ti self-diffusion, even diffusing faster than oxygen [4, 7]. The aim of this study is to explore the potential of hot isostatic pressing (HIPing) as a practical means of avoiding segregation by utilising diffusion-driven solid-state alloying to obtain a homogenous alloy and a fine lamellar α+β Ti microstructure starting from low-cost blended elemental (BE) commercially pure (CP) Ti and Fe powders.

Conventionally temperatures well above the β transus (of pure Ti) have been used to create a chemically homogenised titanium alloy [8, 9, 14, 16, 17], which leads to millimetre sized equiaxed β grain formation that transform to an α lath structure embedded in the large β grains upon cooling with reduced strength and ductility [3, 12, 18]. Solid-state alloy diffusion has been studied for various fast diffusing β stabilizing element added to the Ti–Al system by Teramae et al. [19] from the perspective of understanding martensitic structures. This work was principally concerned with additively manufactured α+β titanium alloys but focused on sintering a mixture of Ti, Al and isotropic β-stabilising powders including Fe at 1000°C. Their work showed significant levels of TiFe intermetallic. Salmasi et al. [13] determined the diffusion kinetics of Fe in Ti at 900°C and 1000°C by making diffusion couples of solid Ti bonded to Fe powder using field-assisted sintering technology (FAST). This work found that even after 1 h, the Fe had diffused around 250 μm into the Ti, giving rise to an extended (~50 μm at 900°C and ~100 μm at 1000°C) zone of β-Ti accompanied by a narrow (~4 μm at 900°C and negligible at 1000°C) TiFe phase region where the Fe concentration drops abruptly.

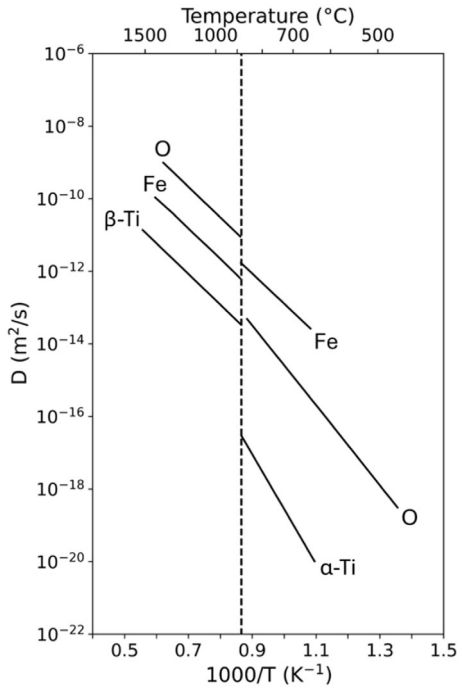

FIGURE 2 | Arrhenius diagram of diffusion coefficient for Ti, Fe and O in the β and α phases of titanium adapted from [3].

Here, we examine the potential to HIP and homogenise a Ti/Fe powder mixture at low temperatures taking advantage of the unusually high diffusion kinetics of Fe in α-Ti with the aim of forming attractive α+β microstructures while restricting excessive β grain growth [14, 16] by homogenising at low temperature (800°C). HIPing is also an interesting manufacturing method from the point of view that it enables to produce a near-net shape product after which only minor machining is required for finished product, which potentially lowers the cost and rejects from machining issues [20]. Further, HIPing is also used to close porosity in additive-manufactured components [21, 22] and hence has the potential of eliminating Kirkendall porosity arising from the vast difference in diffusion kinetics between Fe in Ti and Ti self-diffusion. As a solid-state processing route, HIPing should be conducted below the eutectic temperature to avoid liquid forming.

Critical to this objective is the need to explore the inter-diffusion of Ti–Fe during HIPing and to tailor the microstructure accordingly. To this end, a mixture of Ti-5Fe (wt.%) powders was first consolidated by HIPing at 800°C (i.e. below the β transus of CP Titanium). The subsequent inter-diffusion of the Ti and Fe has then been followed by interrupted homogenising heat treatment at 800°C to allow 3D timec-lapse computed micro-tomography (μ-CT) [23] non-destructively on 1 sample and in parallel by destructive scanning electron microscopy (SEM)/energy dispersive spectroscopy (EDS)/electron backscatter diffraction (EBSD) analysis of a series of (twin sister) samples homogenised for similar times. The partitioning of Fe has also been studied during cooling in situ by EDS within the SEM. In addition, the potential to avoid Kirkendall porosity through additional HIP processing is also investigated.

In this manner, we have shown that difficult-to-cast alloys can be formed by relatively low temperature solid-state processing with favourable microstructures for systems where at least one of the elements is fast diffusing.

2 | Experimental Procedures

2.1 | Hot Isostatic Pressing of Ti-5wt.%Fe

CP titanium (Grade 1) powder with a size distribution between 15 μm to 45 μm was provided by Carpenter Additive, while

TABLE 1 | The size distributions for the powders used in this work. Dv(10), Dv(50), Dv(90) particle sizes corresponding to the 10%, 50%, 90% percentiles of the respective particle size distribution.

Powder	Supplier	Powder size	Dv, 10	Dv, 50	Dv, 90
CP-Ti (Grade1)	Carpenter additive	15–45 μm	21.9 μm	33.5 μm	50.8 μm
99.0% Fe	Goodfellow	<60 μm	18.9 μm	34.7 μm	61 μm

99.0 wt.% pure iron powder with a powder size below 60 μm was provided by Goodfellow metals (Table 1). The size distributions of the Ti and Fe powders were characterised by the laser diffraction particle size analyser (Malvern MasterSizer 3000), and the results are summarised in Table 1. The two elemental powders were mixed in the proportion 95 (Ti) : 5 (Fe) wt.% by vibration mixing over 4 h under an argon protective environment in a custom-made vibration mill. A mild steel canister (25 mm in diameter, 30 mm in length and 2 mm in wall thickness) was filled with the powder mixture under argon environment followed by degassing at ambient temperature to achieve a pressure in the range of 10^{-7} mbar before sealing by hot crimping the evacuation tube.

HIPing was conducted using an AIP8-45H Hot Isostatic Press. The temperature and pressure were ramped at a rate of 5°C/min to a target temperature of 800°C while the pressure ramped up during this time to 80 MPa. Upon reaching the target temperature and pressure, immediate cooling was applied at a (fast) rate of −15°C/min so that the subsequent inter-diffusion between Ti and Fe could be minimised thereby enabling the microstructural evolution to be followed during subsequent homogenisation, both non-destructively on a single sample by CT and destructively by SEM using a series of twin sister samples homogenised for similar times. To this end, 45 test coupons measuring $4 \times 4 \times 4$ mm^3 were cut from the centre of the as-HIPed Ti-5wt.%Fe sample after removal from the mild-steel HIP canister. The actual temperature and pressure profiles recorded during the 800°C HIPing cycle are shown in Figure 3.

The entrained oxygen content was measured by inert gas fusion method, to be 0.19 wt%. This oxygen content, which is typical for conventional two-phase Ti-alloys, is slightly higher than the maximum nominal oxygen content in CP-Ti (grade 1), i.e. 0.18 wt.%. The extra oxygen could be associated with the iron powder.

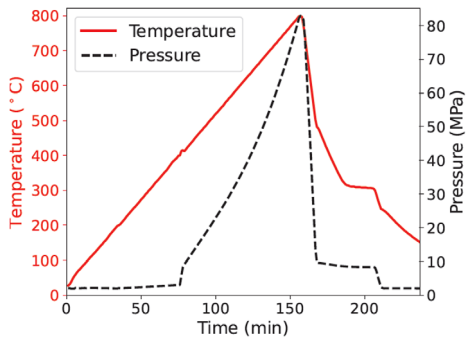

FIGURE 3 | The actual temperature and pressure profiles recorded during the HIPing cycle.

2.2 | Time-Lapse X-ray Computed Tomography (XCT) of Microstructure Evolution during Homogenisation

In order to follow the homogenisation process at 800°C non-destructively, one sample was subjected to a series of heat treatment cycles and examined by time-lapse X-ray μ-CT at room temperature after 0, 1, 3, 6, 9, 12, 15, 21 and 27 h cumulative dwell time at 800°C in argon. The CT scans were acquired on a Zeiss VersaXRM520 x-ray microscope within the Henry Moseley X-ray Imaging Facility at Manchester using an accelerating voltage of 120 kV and 10W power with a LE3 filter. Each scan comprised 1601 projections using a 4X objective lens. An exposure time of 3 s per frame provided sufficient contrast and signal-to-noise ratio for visualisation and segmentation of the phases and porosity, with an effective voxel size of $2.25 \times 2.25 \times 2.25$ μm^3. The different phases were segmented and quantified from the X-ray CT images according to their grey scale range using Avizo 2020 software.

2.3 | Scanning Electron Microscopy

While X-ray CT allows the inter-diffusion process in 3D to be followed on a single sample at temperature, it cannot provide compositional and crystallographic information. To this end, a parallel set of "twin sister" samples were examined destructively at room temperature by SEM, each one corresponding to one of the heat treatment stages recorded by the X-ray CT, i.e. after 0, 1, 3, 6, 12, 15, 21 and 27 cumulative hours of heat treatment at 800°C. In each case, the sample was inserted into a furnace pre-heated to 800°C followed by cooling to room temperature at −1°C/min once the target dwell time had been reached.

For SEM analysis, samples were ground using SiC paper incrementally from grit 600–4000 followed by polishing using a mixture of colloidal silica suspension (0.06 μm) with hydrogen peroxide (of 30% conc) at a volume ratio of 4:1 till the sample surface was scratch-free under an optical microscope. An FEI Sirion SEM was used for imaging and a Tescan Mira3 SEM equipped with an Oxford Instruments Symmetry EBSD detector and X-Max^N 150 EDS detector for EBSD and EDS, respectively. EBSD and EDS scans were conducted using an accelerating voltage of 20 kV. Simultaneous EDS and EBSD were required to separate out the β-Ti and BCC-Fe, which are crystallographically similar. AztecCrystal software was used to reconstruct the parent β-phase grains from the measured room temperature α-phase orientation measurements.

2.4 | Elevated Temperature Scanning Electron Microscopy

A Tescan CLARA SEM with a NewTec FurnaSEM heating stage was used to examine the element redistribution during cooldown from the homogenisation temperature. This Tescan and NewTec

in-situ testing (TANIST) system allows automated tracking, focusing and analysis during the cooling stage (+/−5°C) and is fully described in [24]. An Oxford Instruments UltimMax 170 EDS detector was fitted with an IR filter so that the signal was not washed out by IR radiation emitted from the sample and heater at temperature. A test coupon was heated inside the TANIST to 850°C and held for 12 hr to homogenise and, on cooling, an EDS map was taken every 10°C down to a temperature of 390°C for a total of 46 EDS maps. The EDS maps were acquired with 20 kV, 10 nA, and the map duration was ∼10 min for each map. The average cooling rate of the experiment was 0.8°C/min. Selected frames have been chosen for analysis in the following section, and a video of the entire experiment can be found in the Supplementary Materials.

2.5 | Synchrotron X-Ray Diffraction

Synchrotron X-ray diffraction (XRD) measurements were carried out at room temperature on an as-HIPed sample on beamline I12-JEEP at the Diamond Light Source. The X-ray diffraction signals were collected using a large 2D area diffraction detector (Pilatus 2 M CdTe). A monochromatic beam with a nominal energy of 60 keV was used. X-ray energy and instrument calibration were performed by collecting 2D diffraction patterns on a CeO_2 standard sample at multiple sample-to-detector distances. The beam size was set as 0.5 mm by 0.5 mm. Nineteen diffraction patterns were collected, as the sample was rotated incrementally by 180°. Azimuthal integration of the 2D diffraction pattern was performed using DAWN 2.32 software to get the intensity as a function of q which was subsequently converted to 2θ for Cu Kα radiation. Details of the experimental setup and data processing are presented in [25].

3 | Results

3.1 | Time-Lapse X-Ray CT of Microstructure Evolution during Homogenisation

Figure 4 shows the temporal evolution of the microstructure at a single internal location recorded by X-ray CT during the incremental homogenisation treatment at 800°C, while Figure 5 provides a quantitative assessment of the change in volume fraction of the Fe particles and pores determined over the whole 3D volume by analysing all the segmented virtual CT slices.

It is clear from Figure 4 that the HIPing procedure was sufficient to fully consolidate the powders. The constituent Fe particles can be clearly observed (bright regions), while the grey regions correspond to the consolidated α-Ti. After the first heat treatment cycle (to 800°C with no dwell time), the diffusion of Fe into the Ti at 800°C is evidenced by the light grey contrast surrounding each

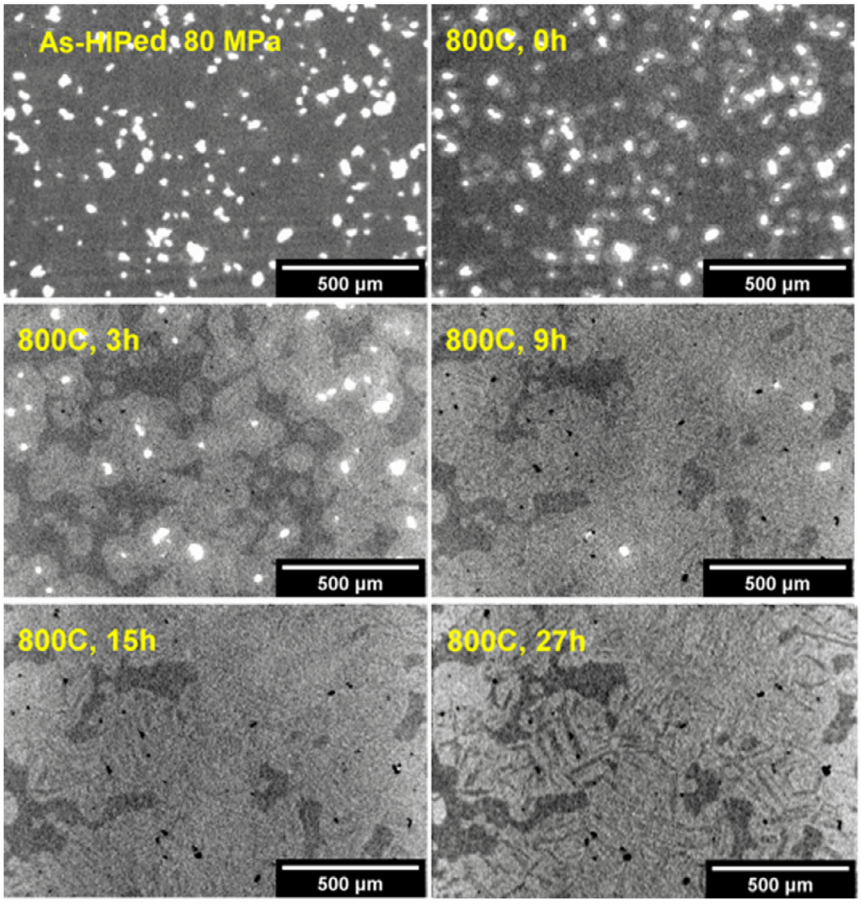

FIGURE 4 | Time-lapse X-ray CT virtual slices acquired at room temperature showing the same central cross-section of the Ti-5wt%Fe sample after different stages of post-HIPing homogenisation (at ambient pressure). The white phase corresponds to Fe, the dark grey phase α-Ti, the light grey phase Fe-rich β-Ti and the darkest phase porosity, as confirmed by destructive SEM EDS/EBSD analysis.

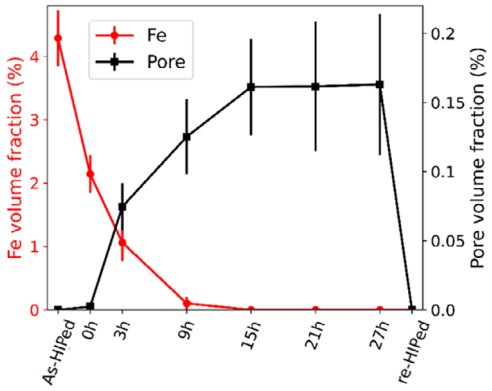

FIGURE 5 | The change in volume fraction of Fe particles and the Kirkendall porosity for the whole ($4 \times 4 \times 4\ mm^3$) volume of the test coupon evaluated from the μ-CT tomograms acquired during post-HIPing 800°C homogenisation at ambient pressure. The error bars represent the standard deviations across the slices.

of the Fe particles. This Fe-rich (β-Ti phase) region extends with further homogenisation until the Fe particles are completely dissolved (after 15 h), after which the growth of the intermediate region appears to have stopped. The alternating bright/dark stripes reflect the formation of an α lath structure within the β which forms during cooling to RT.

The images also reveal an increasing number of pores (dark regions) with heat treatment time, located where the dissolved Fe particles resided in the as-HIPed state. This Kirkendall porosity arises from the very different (five orders of magnitude) diffusion coefficients (see Figure 2) for Fe and Ti giving a net mass flow between the phases [26].

Figure 5 confirms that after 15 h all the Fe particles in the volume have dissolved, while Kirkendall porosity can be seen to increase from the start of the heat treatment peaking at ~ 0.16%, which corresponds to the time at which all the Fe particles had dissolved.

3.2 | Metallographic Observations by SEM

SEM micrographs on polished cross-sections are shown in Figure 6 for samples homogenised to different extents. The as-HIPed sample shows irregularly shaped iron particles within a Ti-matrix, each surrounded by a Fe-rich shell. After 3 h of exposure to 800°C, the Fe-rich shells around the Fe particles have expanded and have started to coalesce. Lamellae are observed in the Fe-rich shells. The lamellar structure disappears towards the residual Fe particles. This has also been observed by Salmasi et al. [13] and is due to the dominance of β phase at high Fe concentrations [27]. After 9 h heat treatment, the Fe particles have dissolved significantly. An extended lamellar microstructure is observed with a few isolated darker (α) regions in between. In common with the CT results in Figure 4, the Fe particles have completely dissolved after 15 h, while regions of α persist.

To confirm the crystallography of the phases in the SEM micrographs and X-ray CT images, EBSD was carried out. The phase maps are shown in Figure 7 for the as-HIPed sample and for the sample homogenised for 15 h. The as-HIPed sample comprises 3 phases: HCP α-Ti (85.6%), BCC β-Ti (7.7%) and BCC Fe (5.1%) with no TiFe or $TiFe_2$ intermetallic phase detected at this resolution (i.e. 0.5 μm step size). The area-weighted mean of the equivalent circle diameter of the grains was 44 ± 16 μm for

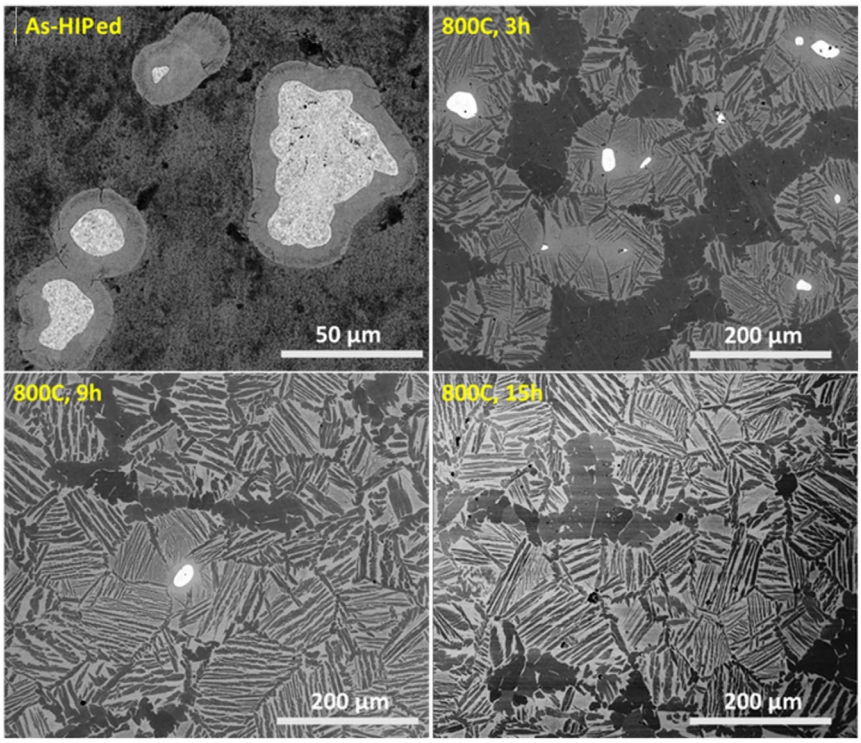

FIGURE 6 | SEM (BSE mode) micrographs showing the microstructure changes during post-HIPing homogenisation for the 'twin sister' samples homogenised under the same conditions as for X-ray μ-CT characterisation shown in Figure 4. The darkest regions phase corresponds to α, the mid grey β and the lightest Fe.

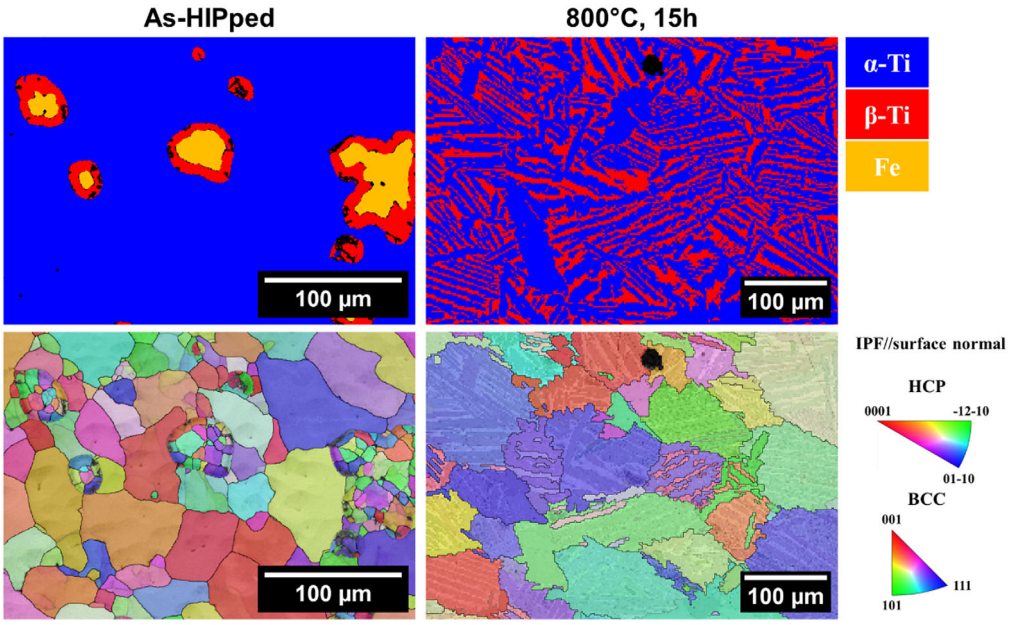

FIGURE 7 | Phase maps (top) and parent β grain reconstruction map (below) obtained from EBSD maps of the HIPed sample and the homogenised sample after heat treatment at 800°C for 15 h. The black regions correspond to regions which were not successfully indexed by the EBSD.

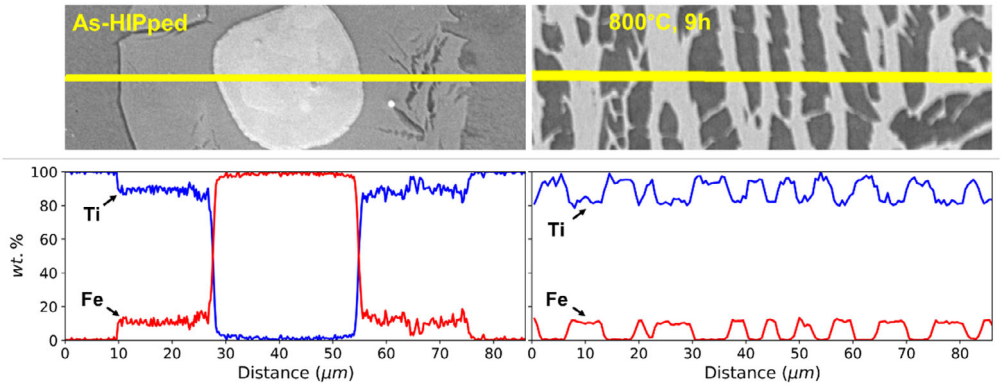

FIGURE 8 | EDS line profiles (bottom) along with BSE regions of interest (top) showing the scan locations (represented by yellow lines) acquired for samples heated to different times.

HCP α Ti, 9 ± 4 µm for BCC β Ti and 14 ± 5 µm for BCC Fe phase. After a cumulative 15 h exposure at 800°C (over 4 thermal cycles), the phase fraction of HCP α and BCC β is 66% and 34%, respectively. The area-weighted mean of the equivalent circle diameter of the reconstructed parent β-Ti grains is 77 ± 26 µm.

To look more closely at the room temperature partitioning of the Fe across the various phases as a function of time at 800°C, EDS line profiles were recorded at room temperature for the twin sister samples along lines that cross-residual Fe particles and the lamellar region in the resultant alloy. The chemical analyses in Figure 8 show the as-HIPed and HIPed + 9 h heat-treated at 800°C condition. In line with the EBSD data, in the as-HIPed condition (Figure 8a), the region previously identified as a β-Ti shell has a Fe concentration ~ 10–12 wt.%, which is close to the eutectoid point in Figure 1. At the interface between the Fe particle and the β-Ti shell, no TiFe or $TiFe_2$ plateau was identified. As mentioned before, previous work creating a Ti–Fe diffusion couple for determining diffusion coefficients of Fe in Ti also found little evidence of significant TiFe or $TiFe_2$ phase [13]. To look more closely at this,

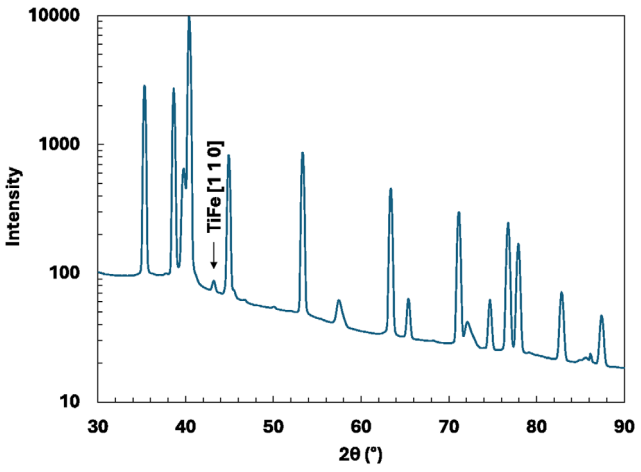

FIGURE 9 | SXRD diffraction profile (summed azimuthally around the whole Debye Scherrer ring) for the as-HIPed material showing evidence of the low level presence of TiFe (note the logarithmic intensity scale).

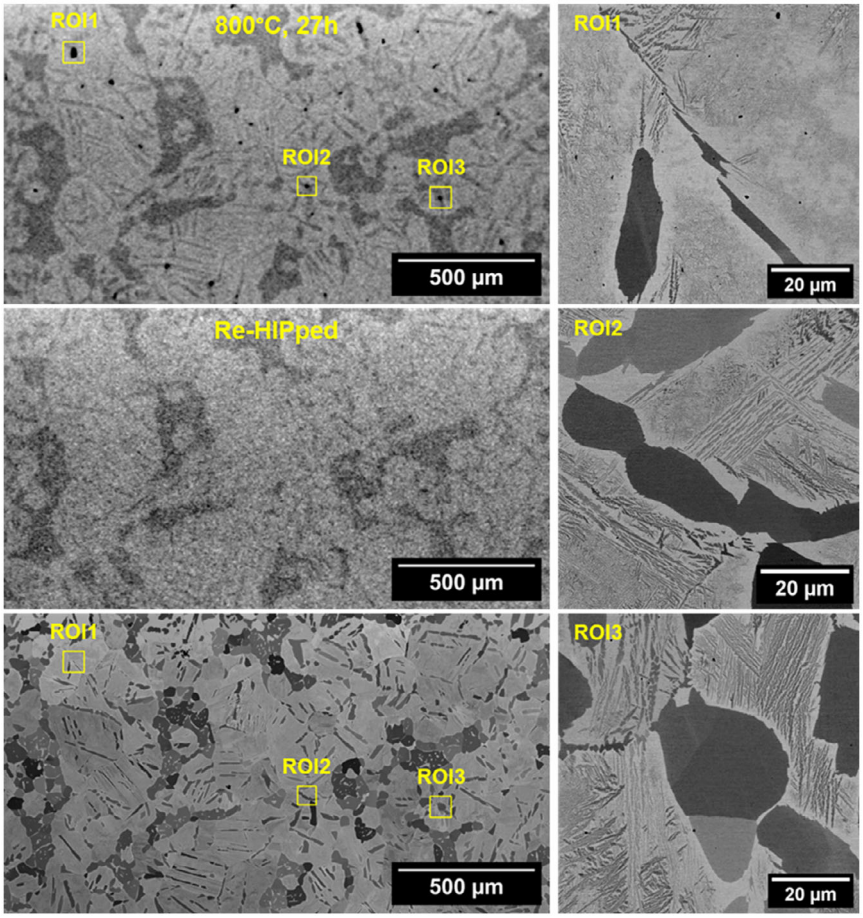

FIGURE 10 | Comparison X-ray CT virtual slices taken before (top left) and after (middle left) the additional HIP cycle and an SEM (BSE mode) micrograph (bottom left) obtained destructively for the same slice. The magnified region of interest SEM images (right) correspond to three locations where Kirkendall pores were originally observed in the CT slice (top left).

high-resolution synchrotron X-ray diffraction (SXRD) analysis on the as-HIPed material reveals a very faint TiFe reflection, Figure 9, confirming that TiFe plays indeed only a very minor role.

3.3 | Kirkendall Defects

A subsequent HIP cycle (at 800°C) at a higher pressure (100 MPa for 3 h) was applied in an attempt to eliminate the Kirkendall pores. Following this, no voids larger than the resolution limit (voxel resolution is 2.25 μm^3) could be detected by X-ray CT (see Figures 10 and 5) suggesting that homogenising under HIP conditions could be used to avoid Kirkendall pores.

Due to the fact that the spatial resolution of X-ray CT is fairly poor, SEM images were also taken of the sample after the additional 3-h HIP cycle. A side-by-side comparison of the XCT virtual slices before and after the additional 3-h HIP cycle and SEM micrography taken on the polished cross-section of the same region is shown in Figure 10. This confirms that micron-scale Kirkendall pores have been successfully removed by the additional HIP cycle.

4 | Discussion

The microstructure of the as-HIPed Ti-5wt.%Fe sample comprises an α-Ti matrix in which each of the Fe particles is surrounded by a very thin TiFe interphase followed by a β-Ti solid solution shell. The shell has formed due to the interdiffusion during the HIPing process. Under the applied pressure and temperature (see Figure 3) during HIPing, the Ti and Fe particles have fully consolidated. The expansion of the β-Ti solid solution shell depends on four processes: (1) the diffusion of Fe from the Fe particle into the β-Ti solid solution shell; (2) the diffusion of Fe through the TiFe interphase, (3) the diffusion of Fe within the β-Ti solid solution shell and (4) the migration of the α/β phase boundary.

At the beginning, the Fe particles sit within a large volume of α-Ti matrix, forming little diffusion couples throughout the material. While the supply of Fe atoms from the Fe particle was abundant, no evidence of $TiFe_2$ and very limited evidence of TiFe were found (see Figure 9). An interesting question that arises from the work here is why this is so, an observation that also agrees with the work in [13]. As Fe is a super-fast diffuser in Ti, it appears that Fe concentration falls sharply across the Fe–Ti interface region such that the Fe content rapidly falls below the 52.5–49.7 at.% corresponding to the intermetallic TiFe phase [5].

Instead of a well-developed TiFe phase, the room temperature analysis shows a β-Ti solid solution shell with a composition close to the eutectoid composition. As the homogenisation proceeded, the Fe particles shrink. According to the Fe–Ti binary

phase diagram (Figure 1), the equilibrium concentration of Fe within the β-Ti solid solution shell at 800°C is ~3.8 wt.%. During cooldown to room temperature, the Fe within the β-Ti solid solution shell near the α/β boundary is not able to fully stabilise the β phase anymore. Consequently, at room temperature, an α+β lamellar structure is developed as shown in Figure 6.

To investigate the details of the Fe partitioning between the phases during cooldown, an in situ EDX mapping study was undertaken in the SEM, and the results are shown in Figure 11. In this study, we increased the homogenisation temperature to 850°C so that the starting microstructure was fully in the β phase region and the Fe distribution homogenous. It is evident that a small amount of α phase has precipitated at 800°C. This is due to the α-stabilising effect of the 0.19 wt.% oxygen present in the sample, as will be discussed later. Further, it indicates that at 800°C the Fe content in the β phase of the α/β is ~ 6 wt.% increasing to around 12 wt.%, as room temperature is approached. The Fe content in the α phase is very low due to almost zero solubility of Fe in the α phase. This illustrates how during cooldown the Fe redistributes towards the receding β phase.

According to the simple Ti–Fe binary phase diagram (Figure 1), the homogenisation temperature used (i.e. 800°C) is above the β-transus temperature for Ti-5wt.%Fe alloy. However, the results of the in situ heating experiment suggest that a small amount of α has started to form by 800°C. This is consistent with the time-lapse X-ray CT results in Figure 4 which shows that the inter-diffusion has stalled after a cumulative homogenisation time of 15 h at 800°C with the residual islands of α phase still evident even after further homogenisation. This is confirmed by SEM observation in Figure 6 for sample homogenised after 15 h. Large islands of α phase can be seen between the α+β lamellar structures.

This is believed to be the result of α-stabilising effect of the (low levels of) oxygen in the as-HIPed sample. To quantify the effect of the 0.19 wt.% oxygen on the phase composition, thermodynamic modelling using CALPHAD was employed to predict the phase composition of the alloy with and without oxygen. The modelling was performed with Thermo-Calc 2019 software using the TCTI2 database. The predicted phase fractions as a function of temperature for the alloy with and without 0.19 wt.% oxygen are compared in Figure 12. For the sample containing 0.19 wt.% oxygen, we would expect 20 mol.% (equivalent to 20 vol.% assuming same molar density for the α and β phase at 800°C) of α phase to coexist with the β phase at 800°C. The α islands observed by XCT and SEM are ≈18.2 vol.% and 15.7 vol.%, respectively.

The eutectoid composition within the β-Ti shell means this phase is expected to be stable during cooling to around 600°C. Below that temperature, one would expect decomposition of the eutectoid β-Ti into α-Ti and TiFe, similar to the pearlite formation in carbon-steel. However, this is not observed here. While Fe is a super-fast diffusing element in Ti, at 600°C, the diffusion coefficient is over an order of magnitude lower than the diffusion coefficient of Carbon in γ-Fe at 723°C. Hence, the low eutectic temperature seems to be responsible for the stabilisation of the β-Ti shell down to room temperature. Previous work with

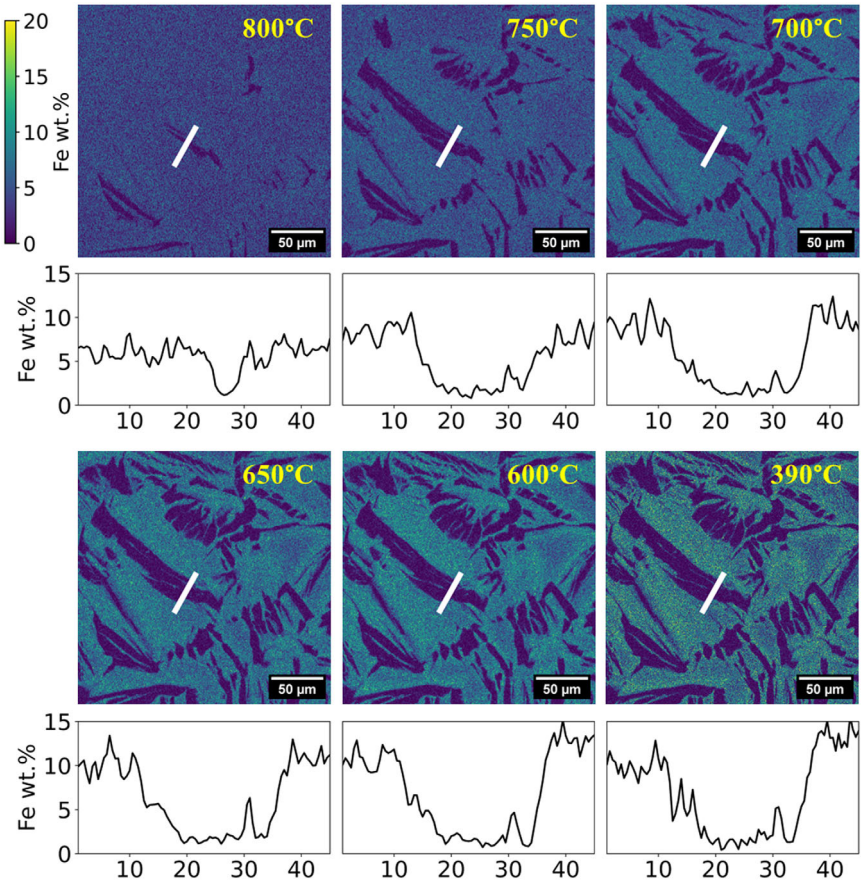

FIGURE 11 | EDS maps (top) and Fe content line profiles (bottom) of the Ti-5%Fe recorded in situ within the SEM as the temperature was lowered from 850°C. A time-lapse video of the entire experiment can be found in the Supplementary Materials.

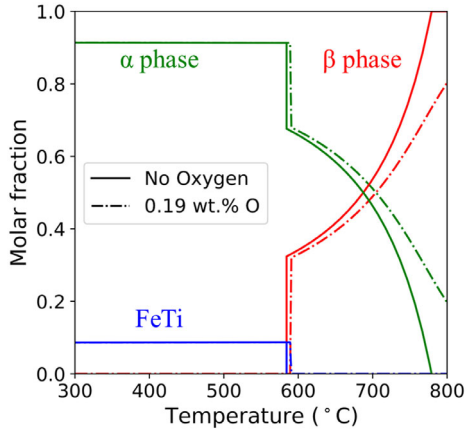

FIGURE 12 | Phase fractions at equilibrium as a function of temperature for Ti-5wt.%Fe alloy both without (solid lines) and in the presence of (dashed lines) 0.19wt% oxygen predicted with TCTI2 v2.1 database in Thermo-Calc Software [7].

the intention of developing β-Ti superalloy based on the TiFe phase evolution showed the necessity of ageing such material within the α-Ti–TiFe phase regime in order to obtain TiFe precipitation [10], which was not carried out in the present case. Figure 8b shows that the lamellar microstructure after the 15 h heat treatment at 800°C, well above the α-TiTiFe phase regime, again shows an eutectoid composition of the β-ligaments without any indication of a eutectoid decomposition.

The small β-Ti grain size (i.e. 77 μm) is a notable aspect of the homogenised microstructure. Conventional α+β Ti-alloys typically display prior β-grains after a β-heat treatment of more than 500 μm. However, such heat treatments are normally carried out above 1000°C due to their high β-transus temperatures. In the present case, as a very strong β-stabiliser, 5 wt.% of Fe lowers the β transus to around 800°C. At such low temperatures, Fe can still diffuse into the Ti matrix fast enough, while the β grain growth has been strongly restricted. The α islands may also help to restrict β grain growth.

Moreover, SEM images do not show any evidence of any significant prior-β grain boundary α phase formation, which are typically soft microstructural features in lamellar microstructures of α +β Ti-alloy. Further no β flecks are observed. Overall, the resulting microstructure promises an excellent balance in mechanical properties between good strength, fracture toughness and reduced crack propagation rates, which will be explored in future studies.

The current samples were too small for mechanical testing. Subsequently, we have since produced a new batch of samples using larger HIP cans using a slightly higher HIP temperature (900°C, above the β-transus) to eliminate Kirkendall pores and obtain a fully lamellar α+β microstructure. TEM characterisation and uniaxial tensile testing revealed the presence of an incommensurate ω phase within the β ligaments in both alloys [28], consistent with previous reports on Ti–Fe systems [27, 29]. The incommensurate ω phase probably contributes to the increased strength but reduced ductility, with both alloys exhibiting a higher yield and ultimate tensile strengths but lower uniform elongation compared with the benchmark CP-Ti. The Ti-2wt.%Fe alloy was less adversely affected and showed superior fracture toughness relative to Ti-5wt.%Fe, likely due to its lower β fraction and reduced ω content. A separate manuscript summarising the microstructure and mechanical property relationships and alloy design implications for these alloys is currently in preparation [28].

5 | Conclusions

We have shown that novel difficult-to-cast alloys can be produced by diffusion-driven solid-state HIP processing of BE powders in cases where one of the elements is a fast diffuser. In our case, Ti-5 wt.% Fe alloy, having an essentially homogeneous α+β, untextured, microstructure, has been produced by co-HIPing Fe and Ti particles. The time-lapse X-ray CT experiment has enabled the tracking of the inter-diffusion of Fe and Ti from the as-HIPed state during homogenisation at 800°C (just below the β transus).

The main findings are as follows:

1) Fully dense Ti-5wt.%Fe alloy can be manufactured by HIPing elemental powers of CP-Ti (Grade1) and 99.0 wt.% Fe under a peak temperature of 800°C and pressure of 80MPa;
2) The as-HIPed alloy (composite) comprises Fe particles surrounded by a β-Ti solid solution shell embedded within an α-Ti matrix;
3) The residual 0.19 wt.% oxygen in the alloy has increased the β-transus temperature of Ti-5wt.%Fe alloy to above 800°C. While the homogenisation has been conducted just below the β-transus temperature, the diffusion of Fe has been reasonably fast and the Fe re-distribution stabilised after homogenisation for 15 h. The homogenised microstructure comprises a largely α/β microstructure with some remnant α islands. Moreover, the lower homogenisation temperature and the residual α islands at homogenisation temperature helped to constrain the β grain growth;
4) The Fe particles completely diffused into the matrix after homogenisation at 800°C for 15 h. Kirkendall pores formed due to the much higher diffusion rate of Fe into the Ti matrix. It is proposed that these pores could be eliminated by maintaining the HIP pressure while homogenising or by employing a second HIPing treatment at 800°C.

In order to observe the mechanical properties of these attractive α+β microstructures, the reader is directed to our further work [28]. Furthermore, this study opens the way for the making of other novel difficult-to-cast alloys by solid-state HIPing and homogenisation from dissimilar powder mixtures in cases where fast diffusion can be exploited. The time-lapse XCT results and in situ EDS results will serve as basis for the development of image-based CALPHAD-informed phase-field models for the inter-diffusion process [30]. Models of this kind can be used to better understand the kinetics of the inter-diffusion process.

Acknowledgments

This research was supported by MAPP:UK-EPSRC Future Manufacturing Hub Manufacture using Advanced Powder Processes (EP/P006566/1). We acknowledge help from the Royce Translation Centre in Sheffield for conducting the HIPing experiments. We acknowledge Dr. Han Liu for the help with Thermo-Calc Software. Beamtime was kindly provided by

the Henry Moseley X-ray Imaging Facility (HMXIF), which was established through EPSRC grants EP/F007906/1, EP/I02249X/1 and EP/F028431/1, part of the National Research facility in X-ray CT funded through EPSRC grant EP/T02593X/1 and UKRI3067 within the Henry Royce Institute for Advanced Materials, established through EPSRC grants EP/R00661X/1, EP/P025498/1 and EP/P025021/1. Our thanks to Haithem Mansour and Oxford Instruments for the loan of the IR filter used in the high temperature EDS experiments in this work. PJW is grateful to Monash University for hosting his sabbatical stay. The synchrotron XRD was undertaken at the Diamond Light Source under beamtime MG28853−1.

Funding

This work was supported by Engineering and Physical Sciences Research Council (Grants EP/P006566/1, EP/F007906/1, EP/I02249X/1, EP/F028431/1, EP/T02593X/1, EP/R00661X/1, EP/P025498/1, EP/P025021/1, UKRI 3067).

Conflicts of Interest

The authors declare no conflicts of interest.

Data Availability Statement

The data that support the findings of this study are available from the corresponding author upon reasonable request.

References

1. M. Peters, J. Hemptenmacher, J. Kumpfert, and C. Leyens, *Titanium and Titanium Alloys* (John Wiley & Sons, Ltd., 2003), 1.

2. Z. Liang, U. Kattner, K. Choudharry, F. Tavazza, and C. Campbell, "Thermodynamic Assessments of Ti-Al, Ti-Fe, and Ti-Al-Fe Systems With Four-Sublattice Description of Ordered Body-Centered Cubic Phase and Density Functional Theory Data," *Journal of Phase Equilibria and Diffusion* 45 (2024): 732.

3. G. Lütjering and J. C. Williams, *Titanium* (Springer, 2007), 15.

4. D. V. Louzguine, H. Kato, L. V. Louzguina, and A. Inoue, "High-Strength Binary Ti–Fe Bulk Alloys With Enhanced Ductility," *Journal of Materials Research* 19 (2004): 3600.

5. J. L. Murray, "The Fe- Ti (iron-titanium) system," *Bulletin of Alloy Phase Diagrams* 2 (1981): 320.

6. R. J. Van Thyne, E. S. Bumps, H. D. Kessler, and M. Hansen, Defense Technical Information Center, 1952.

7. J.-O. Andersson, T. Helander, L. Höglund, P. Shi, and B. Sundman, "Thermo-Calc & DICTRA: Computational Tools for Materials Science," *Calphad* 26 (2002): 273.

8. R. D. Jones, A. J. Knowles, and W. J. Clegg, "A Binary Beta Titanium Superalloy Containing Ordered-Beta TiFe, Alpha, and Omega," *Scripta Materialia* 200 (2021): 113905.

9. D. V. Louzguine-Luzgin, L. V. Louzguina-Luzgina, H. Kato, and A. Inoue, "Investigation of Ti–Fe–Co Bulk Alloys With High Strength and Enhanced Ductility," *Acta Materialia* 53 (2005): 2009.

10. P. O'Kelly, A. Watson, G. Schmidt, M. Galetz, and A. J. Knowles, "Ti–Fe Phase Evolution and Equilibria Toward β-Ti Superalloys," *Journal of Phase Equilibria and Diffusion* 44 (2023): 738.

11. J. Gussone, K. Bugelnig, P. Barriobero-Vila, J. C. da Silva, U. Hecht, C. Dresbach, F. Sket, P. Cloetens, A. Stark, N. Schell, J. Haubrich, and G. Requena, "Ultrafine Eutectic Ti–Fe-Based Alloys Processed by Additive Manufacturing – A New Candidate for High Temperature Applications," *Applied Materials Today* 20 (2020): 100767.

12. C. H. Ng, M. J. Bermingham, L. Yuan, and M. S. Dargusch, "Towards β-Fleck Defect-Free Additively Manufactured Titanium Alloys by Promoting the Columnar-to-Equiaxed Transition and Grain Refinement," *Acta Materialia* 224 (2022): 117511.

13. A. Salmasi, S. J. Graham, I. Galbraith, A. D. Graves, M. Jackson, S. Norgren, D. Guan, H. Larsson, and L. Höglund, "Mobilities of Ti and Fe in Disordered TiFe-BCC Assessed From New Experimental Data," *Calphad* 74 (2021): 102300.

14. P. G. Esteban, L. Bolzoni, E. M. Ruiz-Navas, and E. Gordo, "PM processing and characterisation of Ti–7Fe low cost titanium alloys," *Powder Metallurgy* 54 (2011): 242.

15. A. Devaraj, V. V. Joshi, A. Srivastava, S. Manandhar, V. Moxson, V. A. Duz, and C. Lavender, "A Low-Cost Hierarchical Nanostructured Beta-Titanium Alloy with High Strength," *Nature Communications* 7 (2016): 11176.

16. J. O'Flynn and S. F. Corbin, "The Influence of Iron Powder Size on Pore Formation, Densification, and Homogenization During Blended Elemental Sintering of Ti–2.5Fe," *Journal of Alloys and Compounds* 618 (2015): 437.

17. Z. Z. Fang, J. D. Paramore, P. Sun, K. S. R. Chandran, Y. Zhang, Y. Xia, F. Cao, M. Koopman, and M. Free, "Powder Metallurgy of Titanium – Past, Present, and Future," *International Materials Reviews* 63 (2018): 407.

18. A. Mitchell, A. Kawakami, and S. L. Cockcroft, "Beta Fleck and Segregation in Titanium Alloy Ingots," *High Temperature Materials and Processes* 25 (2006): 337.

19. T. Teramae, A. Issariyapat, S. Kariya, J. Umeda, and K. Kondoh, "Exploring β Stabilizing Elements of α+β Ti-Al Alloys for Facilitating In-Situ Martensite Decomposition in PBF-LB," *Journal of the Japan Society of Powder and Powder Metallurgy* 72 (2025): 201.

20. A. du Plessis and P. Rossouw, "Investigation of Porosity Changes in Cast Ti6Al4V Rods After Hot Isostatic Pressing," *Journal of Materials Engineering and Performance* 24 (2015): 3137.

21. S. Tammas-Williams, P. J. Withers, I. Todd, and P. B. Prangnell, "The Effectiveness of Hot Isostatic Pressing for Closing Porosity in Titanium Parts Manufactured by Selective Electron Beam Melting," *Metallurgical and Materials Transactions A* 47 (2016): 1939.

22. A. du Plessis and E. Macdonald, "Hot Isostatic Pressing in Metal Additive Manufacturing: X-Ray Tomography Reveals Details of Pore Closure," *Additive Manufacturing* 34 (2020): 101191.

23. P. J. Withers, C. Bouman, S. Carmignato, V. Cnudde, D. Grimaldi, C. K. Hagen, E. Maire, M. Manley, A. Du Plessis, and S. R. Stock, "X-ray Computed Tomography," *Nature Reviews Methods Primers* 1 (2021): 18.

24. A. D. Smith, D. Lunt, M. Taylor, A. Davis, R. Thomas, F. Martinez, A. Candeias, A. Gholinia, M. Preuss, and J. M. Donoghue, "A New Approach to SEM In-Situ Thermomechanical Experiments Through Automation," *Ultramicroscopy*. (2025): 114244.

25. J. Xu, "Towards HIPping of Difficult-to-Cast Ti Alloys through Time-Lapse 3D X-Ray Computed Tomography" (PhD Thesis, Manchester University, 2025).

26. H. Strandlund and H. Larsson, "Prediction of Kirkendall Shift and Porosity in Binary and Ternary Diffusion Couples," *Acta Materialia* 52 (2004): 4695.

27. Y. Zheng, D. Huber, and H. L. Fraser, "Investigation of a Nano-Scale, Incommensurate, Modulated Domain in a Ti–Fe Alloy," *Scripta Materialia* 154 (2018): 220.

28. J. Luo, R. Ghosh, A. Ramezannejad, A. D. Smith, B. K.Shan, J. J. Kruzic, B. Gludovatz, P. J. Withers, and M. Preuss, *Deformation and Failure Mechanisms in Ti–Fe Alloys Manufactured through a Novel Hot Isostatic Pressing Process*," in Preparation. 2026.

29. A. J. Knowles, T.-S. Jun, A. Bhowmik, N. G. Jones, T. B. Britton, F. Giuliani, H. J. Stone, and D. Dye, "A New Beta Titanium Alloy

System Reinforced With Superlattice Intermetallic Precipitates," *Scripta Materialia* 140 (2017): 71.

30. C. Liu, A. Garner, H. Zhao, P. B. Prangnell, B. Gault, D. Raabe, and P. Shanthraj, "CALPHAD-Informed Phase-Field Modeling of Grain Boundary Microchemistry and Precipitation in Al-Zn-Mg-Cu Alloys," *Acta Materialia* 214 (2021): 116966.

Supporting Information

Additional supporting information can be found online in the Supporting Information section.